CHEMISTRY OF MATERIALS

Article

pubs.acs.org/cm

Immobilization of Optically Active Helical Polyacetylene-Derived Nanoparticles on Graphene Oxide by Chemical Bonds and Their Use in Enantioselective Crystallization

Weifei Li, Xuan Liu, Guangyue Qian, and Jianping Deng*

State Key Laboratory of Chemical Resource Engineering, College of Materials Science and Engineering, Beijing University of Chemical Technology, Beijing 100029, China

ABSTRACT: The present study originally created a methodology for immobilizing polymeric nanoparticles on graphene oxide (GO) by chemical bonds, aiming at chiral functionalization of GO and simultaneously improving the dispersibility of polymer nanoparticles. To prepare the novel GO hybrids, GO was first prepared and alkynylated to form an actual comonomer (M_{GO}), in the presence of which acetylenic monomer (M_1) underwent emulsion polymerization in aqueous media with sodium dodecyl sulfate as emulsifier and $(nbd)Rh^+B^-(C_6H_5)_4$ as catalyst. SEM and HRTEM images ascertained the formation of polymeric nanoparticles immobilized on GO (NP_{poly1}/GO). CD and UV−vis absorption spectra demonstrated the optical activity of NP_{poly1}/GO, originated from the chiral helical conformations adopted by the polymer chains constructing the nanoparticles. FT-IR, Raman, XPS, XRD, and TGA techniques were also utilized to characterize the GO hybrids. The as-obtained NP_{poly1}/GO was further used as a chiral additive to perform enantioselective crystallization of L-alanine from racemic alanine. L-Alanine was preferentially induced to crystallize rod-like crystals, according to SEM, CD, and XRD characterizations. The present study provides a versatile platform for preparing GO-derived functional materials, particularly novel chiral materials.

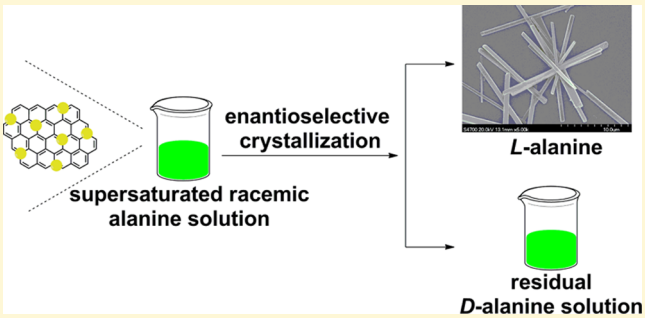

1. INTRODUCTION

Graphene (including graphene oxide, GO) exhibits a series of interesting properties and has attracted much attention in diverse areas, for instance, biotechnology, electronics, capacitors, and advanced composites.[1−5] Up to date graphene-based materials have found exciting applications in fuel cells,[6] actuators,[7] electronics,[8] catalysis,[9−11] adsorbents,[12,13] sensors,[14] membranes,[15] and life sciences.[16] Because of the intractable limitations like poor dispersibility and low reactivity, functionalization of graphene either by chemical bonds or by physical interactions continues to gather growing interest.[17,18] So far, graphene has been elegantly functionalized with DNA,[19] cyclodextrins,[20] amylose,[21] and synthetic polymers,[22] leading to a number of advanced functional materials. Such practices not only afforded graphene with the specifically desirable properties but also improved the dispersibility of graphene.[23] Regretfully, functionalization of graphene with synthetic chiral architectures, in particular artificial helical macromolecules, still remains a big challenge, only with limited success.[24] Such practices will hopefully lead to novel chiral catalysts, chiral sensors, etc. due to the judicious combination of the advantages of both chiral materials and graphene.

Chirality is an intriguing feature of nature. Chiral materials are envisaged as a promising core technology for the health of humans, well exemplified by the widely recognized importance of chiral drugs. Accordingly, intensive efforts have been made in designing and preparing novel chiral (macro)molecules and the materials thereof. Chiral helical polymers are of special interest due to chiral amplification effects.[25,26] Artificial helical polymers have constructed a promising research area, in which the past decade has witnessed fast developments,[27−37] prominently stimulated by the beautiful helical structures formed in biomacromolecules (e.g., proteins and DNA) and their essentially important functions in organisms. More noticeably, the studies from other groups and from us demonstrated the significant potential applications of helical polymers and the particles thereof in such significant areas as asymmetric catalysis,[38−40] chiral recognition/separation,[41] enantiomer-selective crystallization,[42] and chirally controlled release.[43] Also remarkably, chiral helical polymers have been successfully combined with magnetic Fe_3O_4 particles[44] and silica,[45] resulting in some attractive materials.

Even though synthetic helical polymers have largely advanced, they have been scarcely employed to functionalize graphene (oxide). Accordingly, it remains an essential challenge to efficiently combine synthetic helical polymers with graphene. Earlier, we prepared a series of optically active nanoparticles derived from helical substituted polyacetylenes.[46] The nano-

Received: January 20, 2014
Revised: February 18, 2014
Published: February 20, 2014

   dx.doi.org/10.1021/cm500211s | Chem. Mater. 2014, 26, 1948−1956

Scheme 1. Schematic Illustration of the Strategy for Preparing (A) Alkynylated Graphene Oxide (M_{GO}) and (B) the Hybrid Material NP_{poly1}/GO, Which Was Used for Enantioselective Crystallization of L-Alanine (C)

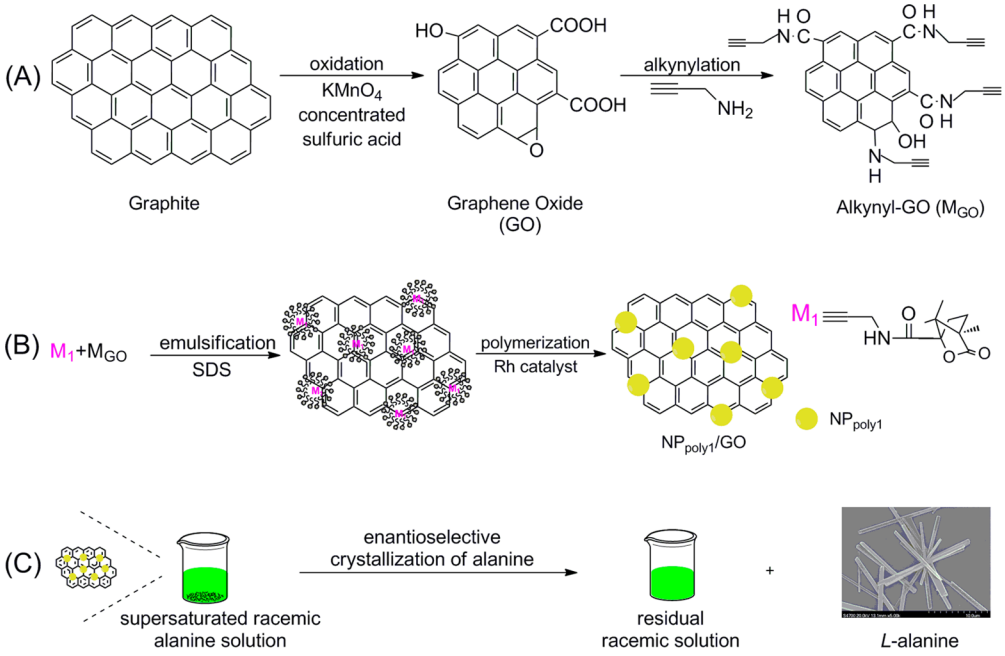

particles, once obtained in pure state, are somewhat difficult to satisfactorily disperse again in solvents. In a later study,[47] we successfully attached chirally helical polymer chains to graphene by physical interactions and created a powerful platform for developing chiral materials based on graphene. To overcome the aforementioned problem (redispersibility of nanoparticles) and to develop novel chiral materials, we in the present study immobilized optically active polymer nanoparticles on graphene oxide (GO). The major objectives include (1) to functionalize GO with optically active polymeric nanoparticles, rendering GO with optical activity; (2) to improve the dispersibility of GO by organic polymeric nanoparticles; and (3) to enhance the dispersibility of the nanoparticles by using GO as carrier. The obtained GO composite was further utilized as a unique chiral additive to accomplish enantioselective crystallization[48,49] by using D- and L-alanine as model chiral compounds. The relevant strategy in the present study is illustrated in Scheme 1.

It should be pointed out that there have been reports dealing with combining polymeric particles onto graphene and GO sheets; however, all the combinations were realized by physical interactions rather than covalently chemical bonds. The specific driving forces include electrostatic interaction[50,51] and thermodynamics.[52] GO sheets were also utilized as special emulsifiers to stabilize polymer particles through emulsion polymerizations.[53−55] Our present study provides a novel strategy, which largely distinguishes from the processes in literature.[50−55] Namely, the optically active polymer particles were tethered on GO sheets by chemical bonds. Also remarkably, the unique optical activity of the resulting GO composites makes them attractive as novel chiral materials.

2. EXPERIMENTAL SECTION

2.1. Materials. $(nbd)Rh^+B^-(C_6H_5)_4$ was prepared according to a procedure reported earlier.[56] Monomer M_1 (structurally presented in Scheme 1) was synthesized according to the literature.[57] Propargylamine, isobutyl chloroformate, *N*-methylmorpholine, dicyclohexylcarbodiimide (DCC), and 4-dimethylaminopyridine (DMAP) were purchased from Aldrich and used without further purification. Graphite powder (300 mesh, 75−82% C, 18−25% ash) was purchased from Alfa Aesar. Potassium permanganate ($KMnO_4$), hydrogen peroxide solution (H_2O_2, 30%), hydrochloric acid (HCl), 96% sulfuric acid (H_2SO_4), and NaOH were commercially obtained. Alanines (D- and L-) were purchased from Aladdin Company (Shanghai, China) and directly used.

2.2. Measurements. Circular dichroism (CD) and UV−vis absorption spectra were conducted on a Jasco-810 spectropolarimeter. Specific rotations were measured on a Jasco P-1020 digital polarimeter with a sodium lamp as the light source at room temperature. FT-IR spectra were recorded with a Nicolet NEXUS 670 spectrophotometer (KBr tablet). X-ray diffraction (XRD) analyses were performed with Shimadzu XRD-6000. High resolution transmission electron microscopy (HRTEM) and scanning electron microscopy (SEM) were, respectively, performed on a JEOL J-800 and Hitachi S-4700 electron microscope. Thermogravimetric analysis (TGA) was carried out with a Q50 TGA at a scanning rate of 10 °C/min under N_2. Raman spectra were recorded on a Renishaw inVia-Reflex confocal Raman microscope with an excitation wavelength of 532 nm. XPS surveys were recorded on a EscaLab 250 X-ray photon-electron spectroscope.

2.3. Preparation of Graphene Oxide (GO). Graphene oxide (GO) was prepared with the method reported by Hummers and Offeman with slight modifications.[58] Graphite powder (1.5 g) was added slowly to 60 mL of sulfuric acid in an ice bath under magnetic stirring. Then, $KMnO_4$ (7.5 g) was gradually added to the mixture within 1 h to avoid a sudden increase in temperature. The resulting mixture was kept at 35 °C for 2 h and then gradually diluted with 100 mL of ice water within 30 min on an ice bath (while keeping the temperature below 40 °C). After the dilution was complete, the mixture was magnetically stirred at room temperature for another 2 h. To stop the oxidization reaction above, 200 mL of deionized water and 25 mL of 30% H_2O_2 were added in the reaction mixture. When bubbling ended, the lightly yellow product was subjected to centrifugation, washed with 10% HCl aq solution, and subsequently with water, and finally dried under vacuum, thereby yielding GO.

2.4. Preparation of Alkynyl-GO (M_{GO}). Alkynyl-GO (M_{GO}) was prepared by the alkynylation of GO with propargylamine in the presence of dicyclohexylcarbodiimide (DCC) and 4-dimethylaminopyridine (DMAP) in DMF. In a typical procedure, GO (0.1 g) was dispersed in 50 mL of DMF by 60 min of sonication in a bath

dx.doi.org/10.1021/cm500211s | Chem. Mater. 2014, 26, 1948−1956

sonicator. Then, propargylamine (0.168 g, 2.73 mmol) was added to the GO suspension and dissolved by stirring. DCC (4 g, 20.87 mmol) and DMAP (0.3 g, 2.46 mmol) were gradually charged into the flask within 20 min. The reaction was conducted at room temperature under stirring for 16 h. After the reaction was completed, the suspension was diluted with 30 mL of DMF and filtered over a 0.2 μm PTFE microporous membrane. The obtained M_{GO} was washed thoroughly using DMF with the assistance of sonication and then dried under vacuum overnight. The yield of alkynyl-GO was 46.8% .

2.5. Preparation of NP_{poly1}/GO. Scheme 1 presents a schematic for preparing the GO-based hybrid material (NP_{poly1}/GO) in which chirally helical substituted polyacetylene-based nanoparticles are chemically bonded on GO sheets. The strategy is designed referring to our earlier study on preparing optically active helical-substituted polyacetylene-based nanoparticles via the catalytic emulsion polymerization approach.[45,46] A typical preparation process is briefly stated below. First, M_{GO} (0.1168 g), dispersed in DMF (2 mL) under ultrasonic conditions, was charged in a 100 mL three-neck round-bottomed flask containing deionized water (18 mL). The mixture was stirred at room temperature for 15 min, after which it was sonicated for one more hour. The purpose is to achieve complete dispersion of M_{GO} in water. To form monomer micelles in water, sodium dodecyl sulfate (SDS, 1.003 g, 3.48 mmol) was dissolved in the aqueous system above, in which M_1 (0.1168 g)/DMF (dimethylformamide, 0.5 mL) solution was added to form the monomer emulsion. In this process, GO sheets adsorbed some SDS molecules onto the outer surfaces, especially the graphene edges where anchoring hydrophobic −C≡C groups are present, therein in situ forming micelles containing M_1 molecules. After stirring for 1.5 h, hydrophobic Rh catalyst $[(nbd)Rh^+B^-(C_6H_5)_4]$ and 0.0026 g/DMF (0.5 mL) solution were added dropwise to the system above to initiate the emulsion polymerization of M_1, during which the −C≡C moieties bonded on the GO sheets also took part in polymerization (see discussions below). The emulsion polymerization lasted for 4 h at 30 °C under a nitrogen atmosphere. The resultant polymer emulsion was subjected to centrifugation (20000 rpm, 20 min) to obtain the pure graphene hybrid (NP_{poly1}/GO), followed by washing with THF four times, and then dried under vacuum. The yield of NP_{poly1}/GO was 73.4% .

2.6. Enantioselective Crystallization of Alanine Induced by NP_{poly1}/GO. A typical enantioselective crystallization procedure was performed as follows, referring to our earlier study.[42] The crystallization experiments were carried out with a supersaturated solution of alanine in deionized water. D- and L-alanine (each 300 mg) were added in deionized water (3 mL), and the solution was heated to 35 °C under stirring for complete dissolution. Approximately 3 mg of NP_{poly1}/GO was placed into the racemic D-, L-alanine supersaturated solution above and stirred for about 30 min. The dispersion was left for ambient cooling till room temperature (approximately 25 °C). Seventy-two hours later, the formed crystals were filtrated. After drying, the crystals were subjected to characterization. The residual filtrate was also subject to measurements. For comparison, crystallization of alanines was performed by using M_{GO} as additive in a similar way. Under similar conditions, crystallization was also performed in the absence of any additive.

3. RESULTS AND DISCUSSION

3.1. Preparation and Characterizations of NP_{poly1}/GO. In the present study, we designed and successfully prepared the first GO hybrid material covalently functionalized with chirally helical-substituted polyacetylene-derived nanoparticles via the catalytic emulsion polymerization approach. The aims are to improve the dispersibility of optically active polymeric nanoparticles and meanwhile to chirally functionalize GO with the nanoparticles. The strategy is illustrated in Scheme 1, which consists of two major steps. In the first step (Scheme 1A), GO was first prepared from graphite by a slightly modified Hummers technique and then underwent alkynylation for forming alkynyl-GO (M_{GO}). The purpose of the alkynylation process is to chemically bond polymerizable −C≡C units on GO by using the −COOH and the epoxy functional groups on the GO sheets. In the second step (Scheme 1B), monomer M_1, together with the polymerizable −C≡C units attached on GO, underwent catalytic emulsion copolymerization, leading to the anticipated chirally functionalized GO, i.e., NP_{poly1}/GO. NP_{poly1}/GO is indeed a new type of graphene-based functional material, interestingly integrating GO and the optically active nanoparticles derived from helical-substituted poly1 (poly1: the polymer derived from monomer M_1). Not surprisingly, the dispersibility of the nanoparticles were improved largely due to their attachment on GO as a carrier, while the nanoparticles rendered GO with intriguing optical activity and also improved the dispersibility of GO in organic solvents, as discussed in more detail below.

To preliminarily verify the formation of the designed NP_{poly1}/GO hybrid, the product was characterized by FT-IR spectroscopy, as presented in Figure 1. A comparison among

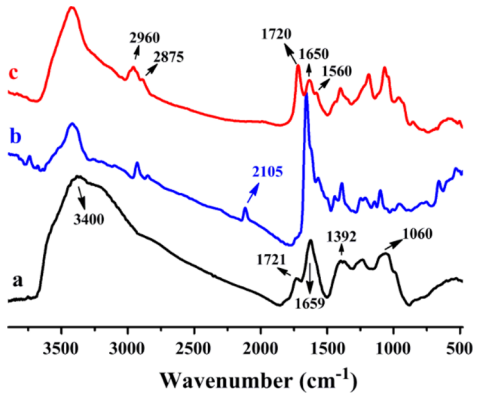

Figure 1. Typical FT-IR spectra of graphene oxide (GO) (spectrum a), alkynyl-GO (M_{GO}) (spectrum b), and NP_{poly1}/GO (spectrum c). The spectra were recorded by using KBr tablet.

the spectra of GO (spectrum a), alkynyl-GO (M_{GO}) (spectrum b), and the final product NP_{poly1}/GO (spectrum c) provides important information. In spectrum a, the absorbance peaks at 1060, 1392, 1659, 1721, and 3400 cm^{-1} are attributed to C−O stretching (epoxy), −OH stretching (carboxylic acid), C═C skeletal vibrations (unoxidized graphite domains), C═O in carboxylic acid moieties, and −OH groups, respectively.

After the alkynylation of GO (M_{GO}), several new peaks appeared on the FT-IR spectrum (spectrum b). The peak at 2105 cm^{-1} indicates the newly introduced −C≡C moieties. The peaks at 1560 and 1650 cm^{-1} indicate the amide (−C(O)NH−) structures, showing the presence of the amide bond formed by reaction between GO and propargylamine, as displayed in Scheme 1. Moreover, the methylene ($-CH_2-$) stretching vibrations at 2960 and 2875 cm^{-1} (spectrum b) are also derived from the process of alkynylation. Spectrum c in Figure 1 demonstrates that, after emulsion polymerization, the −C≡C groups in both M_1 and on M_{GO} were nearly all consumed since the peak at 2105 cm^{-1} (indicating the C≡C structure) completely disappeared when compared to spectrum b. The FT-IR spectra preliminarily confirm the formation of NP_{poly1}/GO.

SEM and HRTEM techniques were subsequently used to directly view the morphology of the original GO and NP_{poly1}/GO at nanoscale. To observe the samples, GO was dispersed in deionized water by sonication, which was then placed on a glass

dx.doi.org/10.1021/cm500211s | Chem. Mater. 2014, 26, 1948−1956

sheet (SEM) and 200 mesh carbon grid (HRTEM), dried, and then observed by SEM and HRTEM. For NP_{poly1}/GO, the emulsion sample was directly placed on a glass sheet (SEM) and on the carbon grid (HRTEM), dried, and then observed by SEM and HRTEM. The typical SEM images are presented in Figure 2 (A and B). A comparison between the SEM images of GO (A) and NP_{poly1}/GO (B) clearly shows the prescence of a noticeable number of nanoparticles in the latter. The nanoparticles are of ca. 470 nm in diameter. In addition, GO sheets in the former underwent pronounced packing, while the GO sheets in the latter existed in dispersed state, indicating the improved dispersibility of GO sheets due to the immobilized polymeric nanoparticles on them.

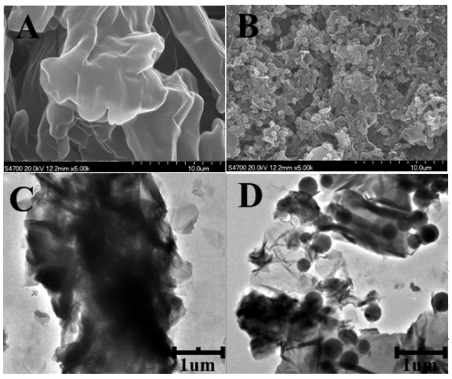

Figure 2. Typical SEM images of GO (A) and NP_{poly1}/GO (B) and HRTEM images of GO (C) and NP_{poly1}/GO (D).

The recorded HRTEM images are illustrated in Figure 2 (C and D). In Figure 2C, GO showed an aggregation morphology, with the exception of some wrinkles derived from the graphene sheets. Compared to it, the HRTEM image for NP_{poly1}/GO in Figure 2D demonstrates clearly the presence of nanoparticles with a diameter of approximately 470 nm. The observations in HRTEM images are similar to the corresponding SEM images discussed above. The nanoparticles in NP_{poly1}/GO are considered as being constructed by the helical polymer chains of M_1 (see below). Both the SEM and HRTEM images definitely verify the occurrence of emulsion polymerization of monomer M_1 and the formation of nanoparticles on the GO sheets. Moreover, the nanoparticles helped to modify the dispersibility of GO in organic solvent, e.g., THF, as depicted in Figure 3.

Without additional dispersant, GO decorated with the poly1-based nanoparticles (NP_{poly1}/GO) became dispersible in THF (Figure 3A). Also, remarkably, the resulting dispersion remained stable, and no obvious precipitation occurred after being stored under ambient conditions for up to one month (Figure 3B). As a sharp contrast, the newly prepared GO could also be dispersed in THF (Figure 3C); however, after storing for just five hours, obvious precipitation took place, as presented in Figure 3D. Accordingly, we in the present study created a facile methodology to not only introduce polymeric nanoparticles onto GO but also improve greatly its dispersion ability in organic solvents.

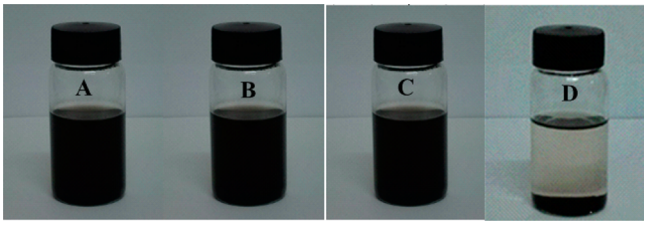

Figure 3. Dispersibility of NP_{poly1}/GO (A,B: 0.025 g) and GO (C,D: 0.025 g) in THF at room temperature. A and C indicate the initial state of the samples, while B and D show the samples after storing for one month (B) and 5 h (D) under ambient conditions.

One of the objectives in the present study is to facilitate GO with optical activity by attaching chirally helical polymer-based nanoparticles, as illustrated in Scheme 1. To confirm the optical activity of the as-prepared NP_{poly1}/GO, the obtained polymer emulsions were characterized by CD and UV−vis absorption spectroscopies, according to our earlier studies dealing with optically active polymeric particles.[39,41−43,46] The relevant CD and UV−vis spectra are shown in Figure 4(A,B). Just as expected, the diluted emulsion showed intense an CD signal and UV−vis absorption around 340 nm. To elucidate the CD and UV−vis spectra, we additionally polymerized M_1 in THF solution (in the absence of M_{GO}) by using the earlier method.[57] The CD and UV−vis absorption spectra of the thus-prepared poly1 homopolymer are also illustrated in Figure 4A and B, in which intense CD and UV absorption also appeared around 340 nm. The intense CD signals and UV absorptions at 340 nm demonstrate the chirally helical conformations formed in poly1 main chains, according to our earlier studies on helical-substituted polyacetylenes both in solution and in particle (nano- and microscaled) states.[45−47] Accordingly, we proposed that the polymer chains constructing the nanoparticles attached on GO sheets (Figure 2B and D) adopted helical conformations with predominantly a one-handed screw sense. The nanoparticles afforded the GO hybrid with the desirable optical activity.

To confirm that the CD effect and UV absorption observed in Figure 4 (A,B) originated from the nanoparticles immobilized on graphene by chemical bonds, pure NP_{poly1}/GO hybrid material should be obtained. For this purpose, NP_{poly1}/GO was first immersed in THF and then subjected to isolation by centrifugation (20000 rpm). Since in the emulsion polymerization of M_1 no specific cross-linking agent was utilized, in theory the nanoparticles composed of only poly1 chains could be removed from GO due to the high solubility of poly1 in THF. However, the −C≡C units preattached on GO may take part in polymerization with M_1, from which the nanoparticles, at least some of them, would not be removed simply by physical means (herein, dissolution and then centrifugation). The hypothesis was proved true, as reported next.

After purification by washing with THF, the as-treated NP_{poly1}/GO sample was subjected to CD and UV−vis spectra measurements. The obtained CD and UV−vis absorption spectra are presented in Figure 5. The NP_{poly1}/GO sample was purified for a total of four times. After the first cycle of separation by centrifugation (Figure 5A and B), both CD and UV−vis spectra of the NP_{poly1}/GO sample showed a pronounced CD effect and UV absorption around 340 nm, while for the corresponding THF solution (the THF filtrate), the CD signal and UV absorption were also strong (Figure 5C and D). The CD and UV spectra recorded in THF solution (Figure 5C and D) indicate that some of the poly1 nanoparticles dissolved in THF, further reflecting these nanoparticles were just physically attached on graphene or

dx.doi.org/10.1021/cm500211s | Chem. Mater. 2014, 26, 1948−1956

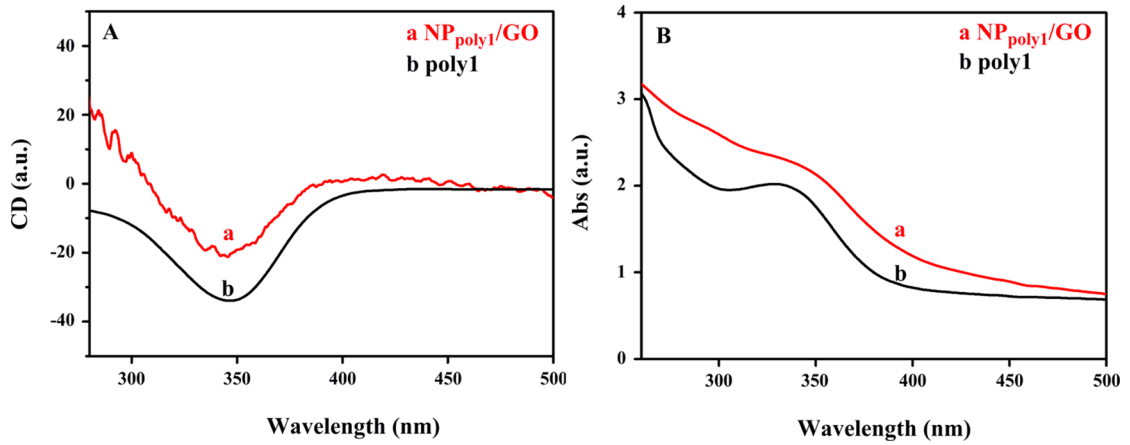

Figure 4. Typical (A) CD and (B) UV−vis absorption spectra of the NP_{poly1}/GO emulsion (0.024 g NP_{poly1}/GO dispersed in 15 mL of water) and poly1 (in THF, M_n = 8000, M_w/M_n = 2.1; 0.1 mM). All of the spectra were recorded at room temperature.

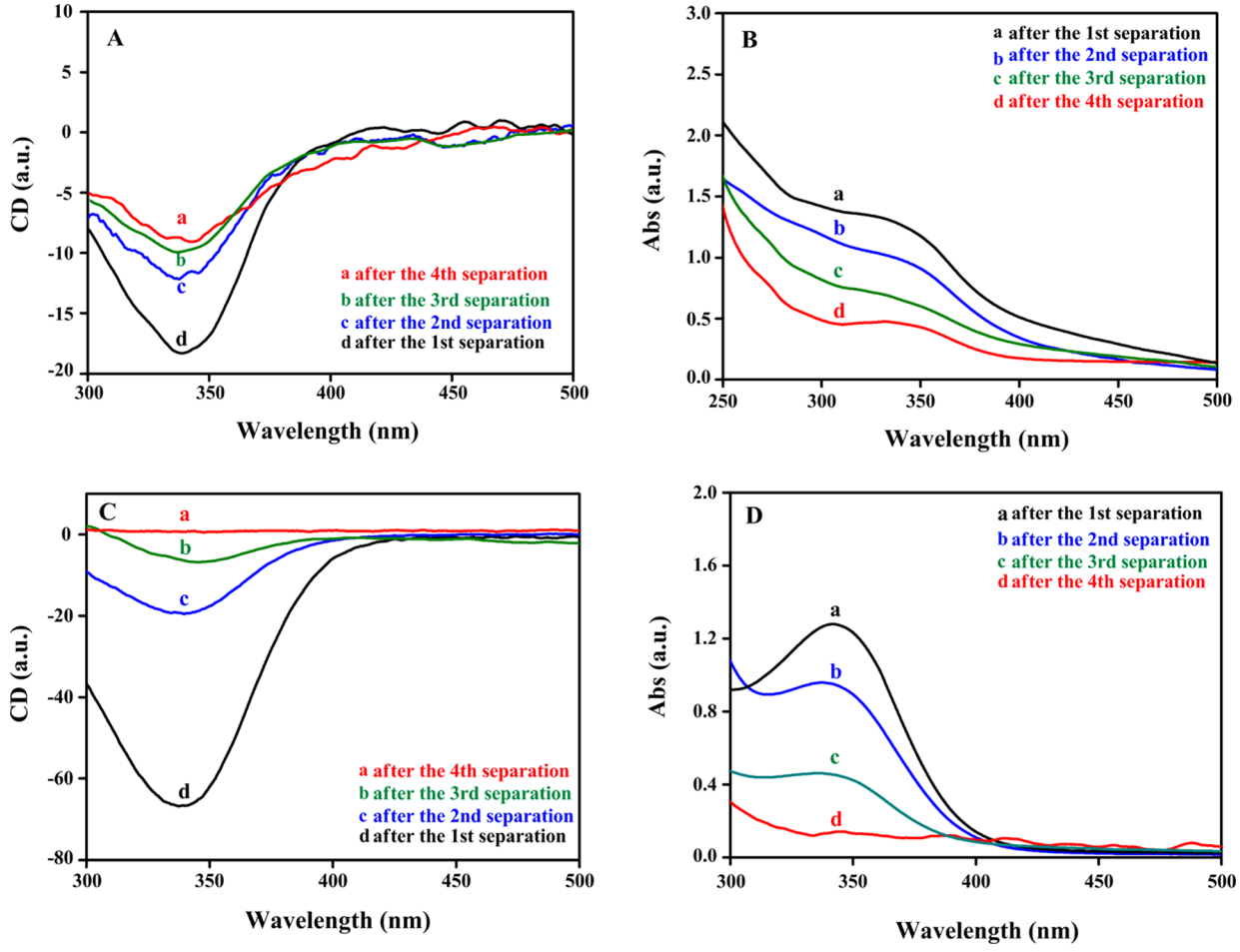

Figure 5. CD and UV−vis spectra of NP_{poly1}/GO (A and B) after purification by washing with THF for four times. C and D present the CD and UV−vis spectra of the corresponding THF solution in each washing cycle. All of the spectra were recorded at room temperature.

formed in the form of free nanoparticles in the resultant polymer emulsion system.

When the NP_{poly1}/GO sample was purified with THF twice and three times, the CD signal and UV absorption for both NP_{poly1}/GO (Figure 5A and B) and THF solution sample (Figure 5C and D) weakened to a certain degree. After washing for four times, the solid NP_{poly1}/GO sample still presented a rather intense CD signal and UV absorption, while no CD and UV absorption could be observed in the corresponding THF filtrate. The observation strongly shows that after purification four times, a remarkable number of poly1 nanoparticles still remained on GO. After that, if the sample was centrifuged for further purification, little change could be observed in the CD and UV−vis spectra in both the NP_{poly1}/GO sample and THF solution. This observation, together with the CD and UV−vis spectra (Figure 4) and the SEM/HRTEM images (Figure 2),

dx.doi.org/10.1021/cm500211s | *Chem. Mater.* 2014, 26, 1948−1956

convincingly demonstrates that optically active nanoparticles were chemically bonded on GO. This also justifies our strategy presented in Scheme 1. Herein, it should be pointed out that the $\pi-\pi^*$ and $n-\pi^*$ transitions of carbon−carbon bonds in GO made the UV absorption (λ, 250−350 nm, Figures 4B and 5B) quite complex.

To acquire more insights into the novel GO hybrids, we next performed X-ray photoelectron spectroscopy (XPS) characterization on the samples, and the recorded spectra are illustrated in Figure 6. Before the test, the samples were washed by excess

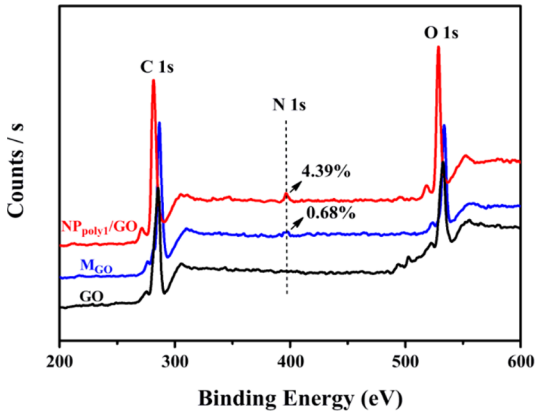

Figure 6. XPS spectra of GO and NP$_{poly1}$/GO.

THF and dried at 50 °C for 72 h, then subjected to measurement. In Figure 6, no N element was detected in the pristine GO. For the alkynylated M$_{GO}$, it exhibited one peak at 406 eV, indicating N 1s and that the content of the N element was 0.68%. For the sample NP$_{poly1}$/GO, N atomic percentage drastically increased to 4.39%, to which the in-situ-formed substituted polyacetylene nanoparticles (primarily derived from M$_1$) largely contributed. This, in combination with other characterizations, strongly reflects that a relatively large quantity of polymer nanoparticles was bonded on GO. We are convinced that after a further optimization in the parameters for performing emulsion polymerization of M$_1$, much more nanoparticles will be attached on GO.

The GO and NP$_{poly1}$/GO prepared above were further subjected to X-ray diffraction (XRD) analysis. The XRD patterns are shown in Figure 7. In the case of GO, there is a sharp reflection peak at 2θ = 10.37° in the XRD pattern, reflecting an interlayer spacing (d) of 0.86 nm, in good

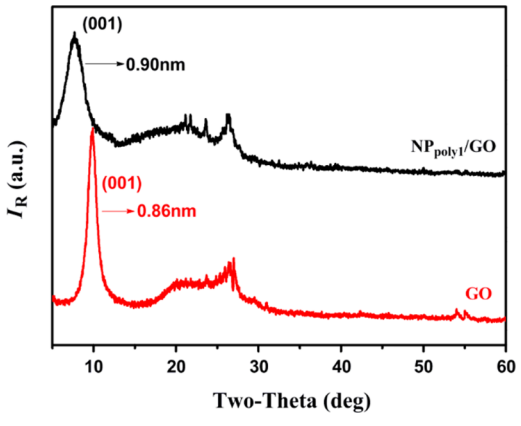

Figure 7. Typical X-ray diffraction pattern of GO and NP$_{poly1}$/GO.

agreement with our earlier study.[47] For NP$_{poly1}$/GO, it exhibited one peak (001) at a lower value (2θ = 9.82°). This shows that the interlayer distance in GO only slightly increased (interlayer spacing, ca. 0.90 nm) compared to that of the pristine GO. It further suggests that the nanoparticles were predominantly immobilized on the surfaces and on the edges of GO. Additionally, the XRD patterns of both GO and NP$_{poly1}$/GO exhibited only one sharp peak (001), suggesting that highly oxidized GO was prepared in the present study.

The ratio between carbon atoms with sp^2 and sp^3 hybridization in the graphene lattice reflects the degree of oxidation or a covalent functionalization occurring to graphene. In the present study, we determined the ID/IG ratio by using Raman spectroscopy. Herein, ID and IG are the intensities of the peaks at ∼1350 and 1590 cm^{-1}, corresponding to the number of sp^3 and sp^2 C atoms, respectively.[59] The obtained Raman spectra are displayed in Figure 8, in which we can

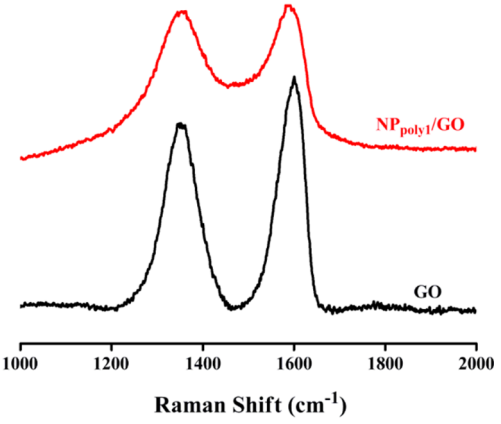

Figure 8. Raman spectra of GO and NP$_{poly1}$/GO.

observe that the ID/IG ratio increased from 0.80 (GO) to 1.13 (NP$_{poly1}$/GO). The increase in ID/IG suggests a decrease in the average size of sp^2 domains in the modified GO sheets.[60]

The thermal stability of the prepared NP$_{poly1}$/GO was also examined by the TGA technique. Analyses were performed from ambient temperature to 800 °C at a heating rate of 10 °C/min under a nitrogen atmosphere. For comparison, both GO and pure poly1 were also tested by TGA. The results are presented in Figure 9. In both GO and NP$_{poly1}$/GO, the oxygen-containing functional groups on the surface began to burn at a temperature of about 190 °C. The remaining fraction of nonvolatile material left at a temperature of up to 800 °C. The helical polymer does not contain any volatile products and therefore began to burn at approximately 250 °C, indicating that the polymer main chains decomposed around this temperature. In NP$_{poly1}$/GO, it lost ca. 14 wt % in the temperature range from 250−475 °C, demonstrating that approximately 14 wt % of poly1-constructed nanoparticles is attached on GO.

3.2. Enantioselective Crystallization of Alanine Induced by NP$_{poly1}$/GO. With the novel chiral material NP$_{poly1}$/GO in hand, we next utilized it as a specific chiral additive for performing enantioselective crystallization,[48,49] by taking alanine as the model chiral compound. We found that NP$_{poly1}$/GO preferentially induced L-alanine to crystallize, and we observed the as-obtained alanine crystals by SEM, as presented in Figure 10C. To obtain a deeper understanding of the enantioselective crystallization, crystallization of racemic

dx.doi.org/10.1021/cm500211s | Chem. Mater. 2014, 26, 1948−1956

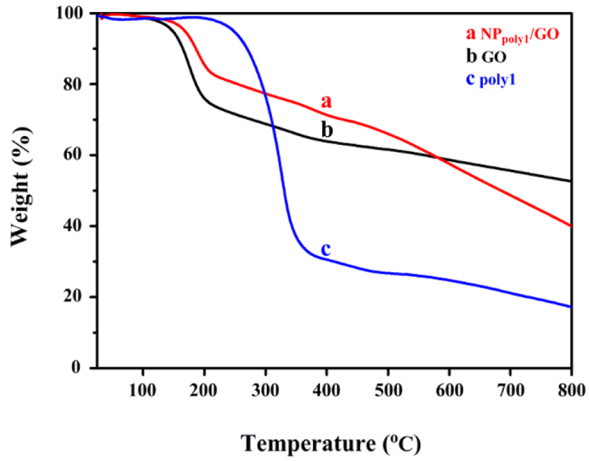

Figure 9. TGA analysis of NP_{poly1}/GO (a), GO (b), and poly1(c) measured at a scanning rate of 10 °C/min under N_2.

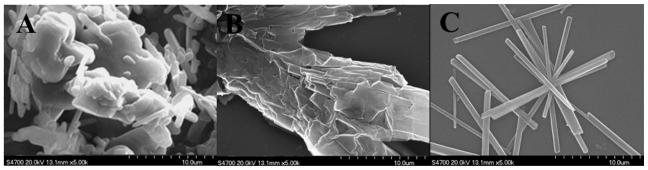

Figure 10. SEM images of alanine crystals obtained via enantioselective crystallization: (A) without additive; (B) by using M_{GO}; and (C) by using NP_{poly1}/GO.

alanine solution was performed under similar conditions but in the absence of any additive. Additionally, M_{GO} was also used as a chiral additive to perform enantioselective crystallization of racemic (D,L)-alanine under the same conditions as those described in the Experimental Section. The SEM images of the alanine obtained via the aforementioned crystallization processes are illustrated in Figure 10. For the alanine crystals obtained without any additive (Figure 10A) and by using M_{GO} as the chiral additive (Figure 10B), powdered solid (Figure 10A) and crystals without regular morphology and size (Figure 10B) were obtained; however, they were confirmed to consist of racemic alanine (the specific rotation was approximately 0°). For the alanine crystals obtained by using NP_{poly1}/GO as the chiral additive, the SEM image in Figure 10C demonstrates beautiful rod-like crystals with regular morphology. Furthermore, the rod-like crystals were experimentally proved to be predominantly constructed by L-alanine, as reported below.

The SEM images in Figure 10 provide evident support for the consideration that the chiral NP_{poly1}/GO was the primary origin of the enantioselective crystallization. Herein, it is important to point out that in our earlier study,[42] enantioselective crystallization of L-alanine was performed by using a chiral helical polyacetylene structurally different from the present M_1-based helical polymer. Therein, the induced L-alanine crystals showed octahedral crystal structure. It seems that the chiral additives largely affected the crystals obtained via the enantioselective crystallization process. Accordingly, more investigations are still required to precisely understand enantioselective crystallization.

The rod-like crystals of L-alanine (Figure 10C) obtained via enantioselective crystallization were subjected to XRD analyses, and the obtained XRD pattern is illustrated in Figure 11, in which the XRD pattern of pure L-alanine is also presented for a vivid comparison. The two patterns are almost entirely the

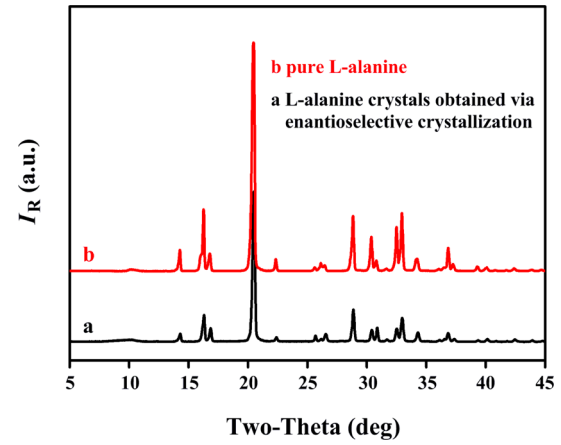

Figure 11. XRD patterens of (a) L-alanine crystals obtained via enantioselective crystallization and (b) pure L-alanine.

same, offering support for the conclusion that the rod-like crystals in Figure 10C are formed predominantly by L-alanine, for which the following characterizations provide further evidence.

The rod-like crystals obtained via enantioselective crystallization was subsequently investigated by CD spectroscopy, as shown in Figure 12. When compared to the pure L-alanine, the

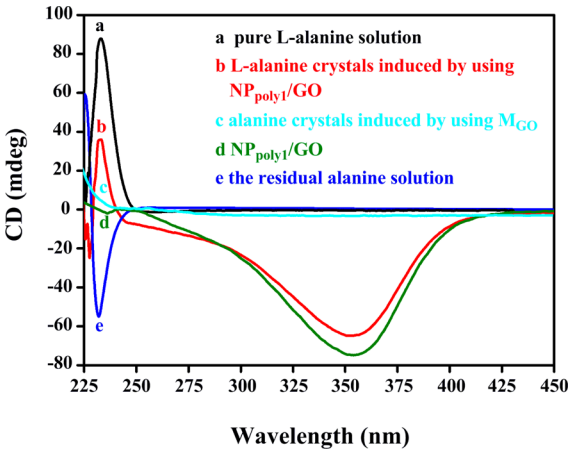

Figure 12. CD spectra of (a) pure L-alanine; (b) L-alanine crystals induced by using NP_{poly1}/GO; (c) alanine crystals induced by using M_{GO}; (d) NP_{poly1}/GO; and (e) the residual solution after removing the L-alanine crystals induced by using NP_{poly1}/GO. All of the CD measurements were performed in aqueous solution at room temperature.

induced L-alanine crystals (in the presence of NP_{poly1}/GO) showed both the CD signals of NP_{poly1}/GO (+, λ_{max} = 350 nm) and L-alanine (+, λ_{max} = 230 nm). To further justify our reasoning, we also measured CD spectra of the alanine crystals obtained by using M_{GO} as the additive and the residual alanine solution after crystallization by using NP_{poly1}/GO as the additive. All of the recorded CD spectra are presented in Figure 12, in which the CD spectrum of NP_{poly1}/GO is also included for a direct comparison. A comparison of the CD spectra in Figure 12 convincingly tells us that the rod-like alanine crystals obtained by using NP_{poly1}/GO as the additive are essentially formed by L-alanine, providing further evidence for the conclusion that enantioselective crystallization was realized by using NP_{poly1}/GO as the chiral additive.

dx.doi.org/10.1021/cm500211s | *Chem. Mater.* 2014, 26, 1948−1956

The chiral resolution efficiency (e.e., enantiomeric excess) in the enantioselective crystallization process was subsequently investigated, as presented in Figure 13. This was accomplished

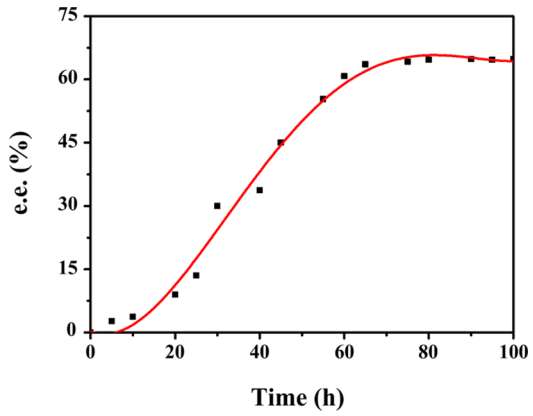

Figure 13. Enantiomeric excess of the residual solution after enantioselective crystallization (D-alanine exceeds in the solution). Enantioselective crystallization of L- and D-alanine, 300 mg, separately, with 3 mL of H_2O and 3 mg of NP_{poly1}/GO.

by measuring the specific rotation of the residual solution as a function of time in the course of enantioselective crystallization.[42,45] Therefore, the e.e. indicates the excessive enantiomer of D-alanine in the residual alanine solution. Figure 13 demonstrates the change of e.e. against crystallization time. It shows that the content of D-alanine in the residual solution gradually increased, further indicating that it was predominantly L-alanine that crystallized forming the rod-like crystals, as discussed above. The maximum chiral resolution was achieved after 72 h, and the e.e. could be as high as 65%. It demonstrates that L-alanine was preferentially induced to crystallize by the NP_{poly1}/GO hybrid.

4. CONCLUSIONS

We have for the first time attached optically active polymer-based nanoparticles on GO by chemical bonds. Such a practice improved the dispersibility of the polymer nanoparticles. Since the nanoparticles were constructed by chirally helical-substituted polyacetylene, they rendered GO with interesting optical activity. Meanwhile, the attachment of polymer nanoparticles also enhanced the dispersibility of GO in organic solvent (e.g., THF). The novel GO hybrid material was achieved via catalyst emulsion polymerization of a substituted acetylene monomer, in the presence of alkynylated GO. The −C≡C groups on GO took part in emulsion polymerization, by which the as-formed polymer nanoparticles were chemically immobilized on the surfaces of GO. Because of the presence of the optically active nanoparticles constructed by helical polymer chains of one predominant screw sense, NP_{poly1}/GO efficiently induced enantioselective crystallization of racemic alanine enantiomers. The success achieved in the present work is far beyond the novel GO hybrid. The present facile approach can be taken as a versatile platform, hopefully extended to other helical and even nonhelical polymers for functionalizing graphene (GO), thereby leading to a number of novel graphene-based advanced materials, in particular chiral materials.

AUTHOR INFORMATION

Corresponding Author

*E-mail: dengjp@mail.buct.edu.cn.

Notes

The authors declare no competing financial interest.

ACKNOWLEDGMENTS

This work was supported by the National Natural Science Foundation of China (21274008, 21174010), the Funds for Creative Research Groups of China (51221002), and the "Specialized Research Fund for the Doctoral Program of Higher Education" (SRFDP 20120010130002).

REFERENCES

(1) Yang, H.; Bachman, R. E.; Feng, X.; Müllen, K. *Acc. Chem. Res.* **2013**, *46*, 116.
(2) Cheng, C.; Li, D. *Adv. Mater.* **2013**, *25*, 13.
(3) Edwards, R. S.; Coleman, K. S. *Nanoscale* **2013**, *5*, 38.
(4) An, X. H.; Simmons, T.; Shah, R.; Wolfe, C.; Lewis, K. M.; Washington, M.; Nayak, S. K.; Talapatra, S.; Kar, S. *Nato Lett* **2010**, *10*, 4295.
(5) Dikin, D. A.; Stankovich, S.; Zimney, E. J.; Piner, R. D.; Dommett, G. H. B.; Evmenenko, G.; Nguyen, S. T.; Ruoff, R. S. *Nature* **2007**, *448*, 457.
(6) Zhu, C.; Dong, S. *Nanoscale* **2013**, *5*, 10765.
(7) Lee, J. S.; Shin, K.-Y.; Kim, C.; Jang, J. *Chem. Commun.* **2013**, *49*, 11047.
(8) Lee, W. H.; Park, J.; Sim, S. H.; Jo, S. B.; Kim, K. S.; Hong, B. H.; Cho, K. *Adv. Mater.* **2011**, *23*, 1752.
(9) Pourazadi, E.; Haque, E.; Zhang, W.; Harris, A. T.; Minett, A. I. *Chem. Commun.* **2013**, *49*, 11068.
(10) Tang, R.; Li, C.; Luo, J.; Kong, Y.; Zheng, W.; Yin, D. *J. Catal.* **2013**, *298*, 138.
(11) Li, J.; Liu, C.; Liu, Y. *J. Mater. Chem.* **2012**, *22*, 8426.
(12) Kemp, K. C.; Seema, H.; Saleh, M.; Le, N. J.; Mahesh, K.; Chandra, V.; Kim, K. S. *Nanoscale* **2013**, *5*, 3149.
(13) Bi, H.; Xie, X.; Yin, K.; Zhou, Y.; Wan, S.; He, L.; Xu, F.; Banhart, F.; Sun, L.; Ruoff, R. S. *Adv. Funct. Mater.* **2012**, *22*, 4421.
(14) Stine, R.; Mulvaney, S. P.; Robinson, J. T.; Tamanaha, Cy R.; Sheehan, P. E. *Anal. Chem.* **2013**, *85*, 509.
(15) Katsnelson, M. I.; Fasolind, A. *Acc. Chem. Res.* **2013**, *46*, 97.
(16) Feng, L.; Wu, L.; Qu, X. *Adv. Mater.* **2013**, *25*, 168.
(17) Kuila, T.; Bose, S.; Mishra, A. K.; Khanra, P.; Kim, N. H.; Lee, J. H. *Prog. Mater. Sci.* **2012**, *57*, 1061.
(18) Georgakilas, V.; Otyepka, M.; Bourlinos, A. B.; Chandra, V.; Kim, N.; Kemp, K. C.; Hobza, P.; Zboril, R.; Kim, K. S. *Chem. Rev.* **2012**, *112*, 6156.
(19) Premkumar, T.; Geckeler, K. E. *Prog. Polym. Sci.* **2012**, *37*, 515.
(20) Liang, R.-P.; Liu, C.-M.; Meng, X.-Y.; Wang, J.-W.; Qiu, J.-D. *J. Chromatogr., A* **2012**, *1266*, 95.
(21) Wei, W.; Qu, K.; Ren, J.; Qu, X. *Chem. Sci.* **2011**, *2*, 2050.
(22) Jiang, K.; Ye, C.; Zhang, P.; Wang, X.; Zhao, Y. *Macromolecules* **2012**, *45*, 1346.
(23) Das, S.; Wajid, A. S.; Shelburne, J. L.; Liao, Y.-C.; Green, M. J. *ACS Appl. Mater. Interfaces* **2011**, *3*, 1844.
(24) Mao, X.; Li, H. *J. Mater. Chem. B* **2013**, *1*, 4267.
(25) Helmich, F.; Lee, C. C.; Schenning, A. P. H. J.; Meijer, E. W. J. *J. Am. Chem. Soc.* **2010**, *132*, 16753.
(26) Green, M. M.; Park, J.-W.; Sato, T.; Teramoto, A.; Lifson, S.; Selinger, R. L. B.; Selinger, J. V. *Angew. Chem., Int. Ed.* **1999**, *38*, 3138.
(27) Jain, V.; Cheon, K.-S.; Tang, K.; Jha, S.; Green, M. M. *Isr. J. Chem.* **2011**, *51*, 1067.
(28) Liu, J. C.; Lam, J. W. Y.; Tang, B. Z. *Chem. Rev.* **2009**, *109*, 5799.
(29) Yashima, E.; Maeda, K.; Iika, H.; Furusho, Y.; Nagai, K. *Chem. Rev.* **2009**, *109*, 6102.
(30) Rudick, J. G.; Percec, V. *Acc. Chem. Res.* **2008**, *41*, 1641.
(31) Pietropaolo, A.; Nakano, T. *J. Am. Chem. Soc.* **2013**, *135*, 5509.

(32) Yoshida, Y.; Mawatari, Y.; Motoshige, A.; Motoshige, R.; Hiraoki, T.; Wagner, M.; Müllen, K.; Tabata, M. *J. Am. Chem. Soc.* **2013**, *135*, 4110.
(33) Freire, F.; Seco, J. M.; Quiñoá, E.; Riguera, R. *J. Am. Chem. Soc.* **2012**, *134*, 19374.
(34) Budhathodi-Uprety, J.; Novak, B. M. *Macromolecules* **2011**, *44* (594742), 913.
(35) Zhang, C. H.; Wang, H. L.; Geng, Q. Q.; Yang, T. T.; Liu, L. J.; Sakai, R.; Satoh, T.; Kakuchi, T.; Okamoto, Y. *Macromolecules* **2013**, *46*, 8406.
(36) Shiotsuki, M.; Sanda, F.; Masuda, T. *Polym. Chem.* **2011**, *2*, 1044.
(37) Jia, H.; Teraguchi, M.; Aoki, T.; Abe, Y.; akaneko, T.; Hadano, S.; Namikoshi, T.; Ohishi, T. *Macromolecules* **2010**, *43*, 8353.
(38) Akai, U.; Yamamoto, T.; Nagata, Y.; Ohmura, T.; Suginome, M. *J. Am. Chem. Soc.* **2012**, *134*, 11092.
(39) Zhang, D.; Ren, C.; Yang, W.; Deng, J. P. *Macromol. Rapid Commun.* **2012**, *33*, 652.
(40) Megens, R. P.; Roelfes, G. *Chem.—Eur. J.* **2011**, *17*, 8514.
(41) Zhou, K.; Tong, L.; Deng, J. P.; Yang, W. *J. Mater. Chem.* **2010**, *20*, 781.
(42) Zhang, D. Y.; Song, C.; Deng, J. P.; Yang, W. *Macromolecules* **2012**, *45*, 7329.
(43) Song, C.; Zhang, C.; Wang, F.; Yang, W.; Deng, J. P. *Polym. Chem.* **2013**, *4*, 645.
(44) Liu, D.; Zhang, L.; Li, M.; Yang, W.; Deng, J. P. *Macromol. Rapid Commun.* **2012**, *33*, 672.
(45) Chen, B.; Deng, J. P.; Yang, W. *Adv. Funct. Mater.* **2011**, *21*, 2345.
(46) Song, C.; Liu, X.; Liu, D.; Ren, C.; Yang, W.; Deng, J. P. *Macromol. Rapid Commun.* **2013**, *34*, 1426 and the references cited therein..
(47) Ren, C.; Chen, Y.; Zhang, H.; Deng, J. P. *Macromol. Rapid Commun.* **2013**, *34*, 1368.
(48) Medina, D. D.; Goldshtein, J.; Margel, S.; Mastai, Y. *Adv. Funct. Mater.* **2007**, *17*, 944.
(49) Menahem, T.; Mastai, Y. *J. Polym. Sci. Part A: Polym. Chem* **2006**, *44*, 3009.
(50) Pham, V. H.; Dang, T. T.; Hur, S. H.; Kim, E. J.; Chung, J. S. *ACS Appl. Mater. Interfaces* **2012**, *4*, 2630.
(51) Zhang, W. L.; Liu, Y. D.; Choi, H. J.; Seo, Y. *RSC Adv.* **2013**, *3*, 11723.
(52) Li, Y.; Wang, Z.; Wang, C.; Pan, Y.; Gu, H.; Xue, G. *Langmuir* **2012**, *28*, 12704.
(53) Thickett, S. C.; Zetterlund, P. B. *ACS Macro Lett.* **2013**, *2*, 630.
(54) Yin, G.; Zheng, Z.; Wang, H.; Du, Q.; Zhang, H. *J. Colloid Interface Sci.* **2013**, *394*, 182.
(55) Das, S.; Wajid, A. S.; Shelburne, J. L.; Liao, Y.-C.; Green, M. J. *ACS Appl. Mater. Interfaces* **2011**, *3*, 1844.
(56) Schrock, R. R.; Osborn, J. A. *Inorg. Chem.* **1970**, *9*, 2339.
(57) Deng, J. P.; Tabei, J.; Shiotsuki, M.; Sanda, F.; Masuda, T. *Macromolecules* **2004**, *37*, 1891.
(58) Hummers, W. S.; Offeman, R. E., Jr *J. Am. Chem. Soc.* **1958**, *80*, 1339.
(59) Yang, Q.; Pan, X. J.; Huang, F.; Li, K. C. *J. Phys. Chem. C* **2010**, *114*, 3811.
(60) Guo, Y.; Guo, S.; Ren, J.; Zhai, Y.; Dong, S.; Wang, E. *ACS Nano* **2010**, *4*, 4001.